ARTICLE

Heterozygous Truncating Variants in *POMP* Escape Nonsense-Mediated Decay and Cause a Unique Immune Dysregulatory Syndrome

M. Cecilia Poli,[1,2,3] Frédéric Ebstein,[4] Sarah K. Nicholas,[1,2] Marietta M. de Guzman,[1,2] Lisa R. Forbes,[2] Ivan K. Chinn,[1,2] Emily M. Mace,[1,2] Tiphanie P. Vogel,[1,2] Alexandre F. Carisey,[1,2] Felipe Benavides,[3] Zeynep H. Coban-Akdemir,[5] Richard A. Gibbs,[5,6] Shalini N. Jhangiani,[6] Donna M. Muzny,[6] Claudia M.B. Carvalho,[5] Deborah A. Schady,[7] Mahim Jain,[5] Jill A. Rosenfeld,[5] Lisa Emrick,[1,8] Richard A. Lewis,[1,5,9] Brendan Lee,[5] Undiagnosed Diseases Network members, Barbara A. Zieba,[4] Sébastien Küry,[10] Elke Krüger,[4] James R. Lupski,[1,5,6,11] Bret L. Bostwick,[1,5,11] and Jordan S. Orange[1,2,*]

The proteasome processes proteins to facilitate immune recognition and host defense. When inherently defective, it can lead to aberrant immunity resulting in a dysregulated response that can cause autoimmunity and/or autoinflammation. Biallelic or digenic loss-of-function variants in some of the proteasome subunits have been described as causing a primary immunodeficiency disease that manifests as a severe dysregulatory syndrome: chronic atypical neutrophilic dermatosis with lipodystrophy and elevated temperature (CANDLE). Proteasome maturation protein (POMP) is a chaperone for proteasome assembly and is critical for the incorporation of catalytic subunits into the proteasome. Here, we characterize and describe POMP-related autoinflammation and immune dysregulation disease (PRAID) discovered in two unrelated individuals with a unique constellation of early-onset combined immunodeficiency, inflammatory neutrophilic dermatosis, and autoimmunity. We also begin to delineate a complex genetic mechanism whereby *de novo* heterozygous frameshift variants in the penultimate exon of *POMP* escape nonsense-mediated mRNA decay (NMD) and result in a truncated protein that perturbs proteasome assembly by a dominant-negative mechanism. To our knowledge, this mechanism has not been reported in any primary immunodeficiencies, autoinflammatory syndromes, or autoimmune diseases. Here, we define a unique hypo- and hyper-immune phenotype and report an immune dysregulation syndrome caused by frameshift mutations that escape NMD.

Introduction

Inborn errors of immunity or primary immune deficiency (PID) are caused by variants in genes encoding molecules relevant to the innate or adaptive immune response. To date, defects in more than 300 different genes have been identified as causes of PID, and heterogeneous clinical manifestations range from increased susceptibility to infection to autoimmunity or autoinflammation.[1–3] All represent aberrant immunity that creates an inability to contend with either the external or internal environment. Within the spectrum of autoinflammatory PID, genetic defects that affect the proteasome have been described as causing autoinflammatory disease and represent a growing area of investigation.[4–8]

The proteasome is the main cellular non-lysosomal proteolytic machinery and is tasked with degrading polyubiquitinated proteins to maintain protein homeostasis. The core particle (or catalytic particle) of proteasome 26S is a cylindrical structure composed of four stacked rings of α and β subunits. Proteasome maturation protein (POMP) serves as a chaperone for proteasome assembly, and whereas other chaperones, namely PAC1 and PAC2 as well as PAC3 and PAC4, participate in early polymerization of the α ring, POMP interacts with an initially formed α ring for subsequent sequential incorporation of β subunits into both the standard proteasome and the immunoproteasome.[9] A half-mer consists of one α ring (α1-7) and a β ring (β1-7) together with PAC1/2 and POMP. Although POMP has not been crystalized, it is predicted to dimerize to participate in the formation of a half-mer and further tetramerize when two half-mers join to form a mature 20S proteasome consisting of two outer α rings and two inner β rings.[10,11] Upon the completion of proteasome maturation, POMP is degraded by the same proteasome.[10,12] The 20S catalytic subunit can then bind to a 19S regulatory subunit and to the interferon (IFN)-inducible activator PA28 to form the 26S hybrid proteasome.[13–16] The β1, β2, and β5 subunits confer the proteasome with caspase-like, trypsin-like, and chymotrypsin-like catalytic activity, respectively, which is needed for processing cellular proteins. Immune cells form a specialized proteasome called

[1]Department of Pediatrics, Baylor College of Medicine, Houston, TX 77030, USA; [2]Texas Children's Hospital, Division of Pediatric Immunology, Allergy, and Rheumatology, Houston, TX 77030, USA; [3]Instituto de Ciencias e Innovación en Medicina, Universidad del Desarrollo, Clínica Alemana de Santiago, RM 7590943, Chile; [4]Universitätsmedizin Greifswald, Institut für Medizinische Biochemie und Molekularbiologie, 17475 Greifswald, Germany; [5]Department of Molecular and Human Genetics, Baylor College of Medicine, Houston, TX 77030, USA; [6]Human Genome Sequencing Center, Baylor College of Medicine, Houston, TX 77030, USA; [7]Texas Children's Hospital, Department of Pathology and Immunology, Houston, TX 77030, USA; [8]Department of Neurology, Baylor College of Medicine, Houston, TX 77030, USA; [9]Department of Ophthalmology, Baylor College of Medicine, Houston, TX 77030, USA; [10]Centre Hospitalier Universitaire de Nantes Hôtel-Dieu, Institut de Biologie, Service de Génétique Médicale, Laboratoire de Génétique Moléculaire, 44093 Nantes Cedex 1, France; [11]Texas Children's Hospital, Houston, TX 77030, USA
*Correspondence: orange@bcm.edu
https://doi.org/10.1016/j.ajhg.2018.04.010.

the i20S immunoproteasome by selectively incorporating specialized β1i (LMP2), β2i (MECL-1), and β5i (LMP7) catalytic subunits. During an immunological challenge, non-immune cells are stimulated by immune response products (IFN-γ or tumor necrosis factor α [TNF-α]), to upregulate i20S and enhance antigen presentation via class I major histocompatibility complex (MHC-I) molecules, allowing for the generation of an appropriate specific T cell response with subsequent T cell expansion and survival.[15,17,18] POMP is also upregulated by IFNs to enhance the incorporation of LMP7 catalytic subunits and accelerate i20S assembly. POMP silencing results in decreased 20S proteasomes, reduced MHC-I antigen presentation, and the induction of apoptosis.[13,19,20]

Autosomal-recessive (AR) biallelic or digenic loss-of-function variants in proteasome subunits have been shown to cause an autoinflammatory syndrome characterized by chronic neutrophilic dermatosis, lipodystrophy, and elevated temperature (CANDLE [MIM: 256040]). This syndrome is associated with increased expression of type 1 IFN and type-1-IFN-inducible genes and was initially described in individuals with mutations in *PSMB4* (MIM: 602177; encodes β7) and/or *PSMB8* (MIM: 177046; encodes β5i) and reproduced by experimental proteasome inhibition in healthy donor peripheral-blood mononuclear cells (PBMCs).[4] Collectively, autoinflammatory syndromes associated with mutations within the proteasome have been referred to as proteasome-associated autoinflammatory syndromes (PRAASs). POMP is required for proteasome maturation in general and the incorporation of LMP7 (β5i) into the i20S.[13] In consideration of the key role of POMP in proteasome assembly, autosomal-dominant (AD) frameshift variants in *POMP* (MIM: 613386) had been suspected to result in PRAASs, but a defect in proteasome assembly had not been confirmed, and any genetic mechanism of POMP-related disease is unknown.[4,8,21] In contrast, AR deletions in the 5′ UTR of an alternative *POMP* transcript give rise to a longer-lived transcript that leads to a keratinization disorder of the skin (KLICK syndrome [MIM: 601952]) with no inflammatory component.[22,23]

Here, we report two unrelated individuals with a neonatal-onset autoinflammatory disease characterized by striking inflammatory neutrophilic dermatosis, autoimmunity, and PID. The disorder is caused by *de novo* heterozygous *POMP* frameshift variants that escape nonsense-mediated mRNA decay (NMD) and result in a truncated protein that disrupts proteasome assembly and leads to increased expression of type-1-IFN-inducible genes.

Material and Methods

Processing of PBMCs

PBMCs were isolated by density centrifugation over Ficoll-Paque media according to the manufacturer's protocol (Amersham). PBMCs were used for the generation of lymphoblastoid cell lines (method described below), stained for flow cytometry, or lysed for western blot assays. All blood samples used for immunobiological analyses were obtained after informed consent for "Genetic and Molecular Investigations in Primary Immunodeficiency" was approved by the Baylor College of Medicine internal review board for the protection of human subjects (H-21453).

Flow-Cytometry Assays

PBMCs were left untreated or stimulated with 1 μg/mL of staphylococcal enterotoxin B (EMD Millipore) plus anti-CD28 and anti-CD49D (BD Biosciences) for 5 hr, washed, and stained for surface markers and intracellular cytokines according to standard procedures. Data were acquired on a modified LSR Fortessa (BD Biosciences) and analyzed with FlowJo X (Tree Star).

Cell Lines

Generation of Lymphoblastoid Cell Lines

Lymphoblastoid cell lines were generated from patient PBMC by transformation with Epstein-Barr virus (EBV)-containing supernatant as previously described.[24] In brief, PBMCs were transduced with a B95-8 EBV cell supernatant and cultured in RPMI medium with 10% FBS, 2 mM glutamine, and 1 μg/mL cyclosporin A. Cell lines were confirmed as mycoplasma negative before their use in experiments using a PCR-based assay (Sigma Aldrich).

Generation of Fibroblast Lines

Patient fibroblasts were obtained from skin punch biopsies, and a primary fibroblast line was derived. Cells were cultured in complete DMEM (high-glucose DMEM, 10% heat-inactivated fetal bovine serum, and 1× GlutaMAX from Sigma Aldrich, Atlanta biological, and GIBCO, respectively) at 37°C with 5% CO_2 and maintained by splitting every 72 to 96 hr at a ratio of 1:3. Viral transformation was performed by Applied StemCell via their standard protocol. For viral transduction, 1×10^5 cells were infected with freshly packaged lentivirus encoding SV40 large T antigen. The cells were selected by puromycin and passaged about five times. Analysis of transgene expression was performed for validation with the following primers: 5′-GGGAGGTGTGGGAGGTTTTT-3′ (SV40 forward) and 5′- TCAAGGCTCATTTCAGGCCC -3′ (SV40 reverse).

Whole-Exome Sequencing Analysis

After informed consent was obtained according to the Baylor-Hopkins Center for Mendelian Genomics (BHCMG) research protocol (institutional review board protocol number H-29697), whole-exome sequencing (WES) was performed on individual A and his parents according to previously described protocols.[25] For individual B, WES was performed clinically first, and research analyses of the clinical exome data were then performed under the BHCMG protocol after informed consent was obtained from the parents. In brief, genomic DNA was extracted from ethylenediaminetetraacetic-acid-preserved non-heparinized blood samples with the Gentra PureGene Blood Kit (QIAGEN). Exonic portions of genomic DNA fragments were captured in solution with VCRome 2.1 design 10 probes (42 Mb NimbleGen, catalog no. 06266380001) according to the manufacturer's protocol (NimbleGen SeqCap EZ Exome Library SR). Resulting DNA was sequenced with Illumina HiSeq 2500 equipment. Data processing and variant annotation were performed per standard pipeline analyses. Variants were evaluated with both recessive and dominant models. Bioinformatic filters were placed with a minor allelic frequency (MAF) less than 0.005 in recessive models within the

BHCMG database, NHLBI Exome Sequencing Project Exome Variant Server (ESP 5400), 1000 Genomes, and the Exome Aggregation Consortium (ExAC) Browser. Potential recessive variants were also excluded if they were present in the ExAC Browser with a homozygote or hemizygote count of ten or greater. For analyses of AD models, variants were excluded if their MAFs were greater than 0.001 in the same databases and if they were present in the ExAC Browser with an allele count greater than five. Variants were confirmed by Sanger sequencing; primers were constructed with Primer3, and amplified DNA constructs were sequenced by the Baylor DNA Sequencing Core Facility. Sequences were visualized with 4Peaks software (Nucleobytes).

RNA Extraction, Sequencing, and Real-Time Quantitative PCR

RNA was extracted from PBMCs or cell lines with the RNeasy Mini Kit (QIAGEN) according to the manufacturer's instructions. The RNA was treated with DNase (QIAGEN) to avoid genomic DNA contamination, and 200 ng of total RNA was reverse transcribed with the SuperScript VILO cDNA Synthesis Kit (ThermoFisher Scientific). The following primers were used for amplifying and sequencing exon 5 of *POMP* from cDNA: 5′-ATGGAATTCAAGG CAGTGCA -3′ (forward) and 5′-AAACCAAAGACCCCTCCAAA-3′ (reverse).

Real-time quantitative PCR (RT-qPCR) experiments were performed in 10 μL reactions with a LightCycler 96 system (Roche) according to the manufacturer's instructions with TaqMan Gene Expression Assays (Life Technologies; primers are further described in the Supplemental Data). GAPDH was used as an endogenous control. Results are based on at least three separate RNA preparations from each cell culture or PBMC sample and two independent RT-qPCR assays for each cDNA synthesis. RT-qPCR samples were run in triplicate and normalized to GAPDH. Data are presented as the mean ± standard deviation (SD) expressed as the relative ratio to GAPDH or, in terms of fold change, to a healthy donor control.

RNA Sequencing

Total RNA was extracted from PBMCs or cell lines with Trizol reagent (Invitrogen). Primary microRNAs and mRNAs were captured by Dynabeads Oligo (dT)25 magnetic beads (Invitrogen) and fragmented with the NEBNext Magnesium RNA Fragmentation Module (New England Biolabs). Double-stranded cDNAs were synthesized with the SuperScript Double-Stranded cDNA Synthesis Kit (Invitrogen) and used as the library template. Libraries were generated with the TruSeq RNA Library Preparation Kit (Illumina). Sequencing was performed on an Illumina HiSeq 2000 instrument with 100 bp pair-end reads at the Human Genome Sequencing Center at the Baylor College of Medicine. Raw reads were mapped with bowtie (v.0.12.7) and Tophat (v.2.0.0) in the strand-specific model when the strand-specific library protocol was applied. The reference genome annotation file was downloaded from the UCSC Genome Browser. Read counts mapped to each gene were calculated by HTseq with the default model. Fragments per kilobase of exon model per million fragments mapped values were calculated with Cufflinks v.2.1.1 and compared with those of 28 whole-blood controls. Visual inspection of *POMP* transcript was performed in Integrative Genomics Viewer (IGV) v.2.4.

Cloning and Transfection of Expression Vectors

A pCMV6-XL5 vector containing the coding sequence of human *POMP* (Origene catalog no. SC114530) was used as a template for the generation of subject-derived mutant variants via site-directed mutagenesis (Epoch Life Science). Wild-type and mutant *POMP* sequences were confirmed by Sanger sequencing of resulting plasmids, which were then transfected into HEK293T cell lines with Lipofectamine 2000 (ThermoFischer Scientific) according to the manufacturer's recommendations. In some experiments, transfection of HEK293T cells with the various *POMP* variants was carried out with the jetPRIME transfection reagent (Polyplus transfection) according to the manufacturer's instructions.

SDS-PAGE, Native Gels, and Western Blot Analysis

Western Blot Analysis

Cells were lysed with 1× Chaps buffer (Cell Signaling Technologies) with protease inhibitor (Thermo). Lysates were run according to standard methods on a 16% Tris-Glycine gel (Novex) and transferred onto a nitrocellulose membrane that was then probed for POMP with actin as a loading control. Antibodies included anti-POMP (D2X9S) rabbit monoclonal, and polyclonal anti-βactin (Sigma). Blots were imaged with an Odyssey imaging system (Li-Cor).

Proteasome Assembly Studies

In western blots for proteasome assembly, equal amounts of RIPA (50 mM Tris [pH 7.5], 150 mM NaCl, 2 mM EDTA, 1% NP40, and 0.1% SDS) or TSDG (10 mM Tris [pH 7.0], 10 mM NaCl, 25 mM KCl, 1.1 mM MgCl2, 0.1 mM EDTA, 1 mM DTT, 1 mM NaN3, and 20% glycerol)-buffered protein extracts from subject EBV-transformed B cells, fibroblasts, or transfected HEK293T cells were separated in SDS-Laemmli gels (15%) or native PAGE gels (3%–12%, Invitrogen), respectively, and western blotted for proteasome subunits as indicated. The RIPA-insoluble fractions derived from subject EBV-transformed B cells and/or fibroblasts were obtained by resuspension of the remaining RIPA-insoluble cell pellets in urea lysis buffer (8 M urea, 2 M thiourea, and 4% CHAPS). The anti-α6 (clone MCP20), anti-α2 (clone MCP21), anti-Rpt6 (clone p45-110), anti-β1 (clone MCP421), and anti-β2 (clone MCP165) primary antibodies were purchased from Enzo Life Sciences. The anti-β1i (LMP2, K221) and anti-PA28-α (K232/1) antibodies are laboratory stocks and were used in previous studies.[15,16] Antibodies specific to Rpn5 (clone H3), β5i (LMP7, clone A12), and β-actin (clone C4) were purchased from Santa Cruz Biotechnology. The polyclonal anti-β2i (MECL1, PA5-19146) and anti-GADD34 (PA1139) antibodies were purchased from ThermoFischer Scientific. The anti-ubiquitin primary antibody (Z0458) was a product of DAKO GmbH. Primary antibodies specific to TCF11/Nrf1 (clone D5B10), eIF2α (#9722), and peIF2α (#9721) were obtained from Cell Signaling Technology. Anti-β5 (ab3390) and anti-α-tubulin (clone DM1A, ab7291) antibodies were purchased from Abcam. The anti-V5 antibody was purchased from Invitrogen (#R960 [1]). Purified 26S proteasomes from erythrocytes (laboratory stock) were used as an internal control.

Immunofluorescence

Staining

Fibroblasts were plated on chambered slides (Falcon) pre-coated with 10 mg/mL of fibronectin (Sigma Aldrich). After 3 hr, cells were fixed with 4% paraformaldehyde with 0.1% Triton X-100 at room temperature and then gently washed with 1% BSA in PBS (all from Sigma Aldrich). Staining for BiP was performed in this buffer with anti-GRP78/BiP (Abcam) and a secondary goat anti-rabbit immunoglobulin G (IgG) conjugated to Alexa Fluor 488, F-actin was labeled with phalloidin Alexa Fluor 568, and the

Table 1. Clinical Summary of Two Unrelated Individuals Studied

Clinical Features	Individual A	Individual B
Sex	male	male
Age of onset	second week of life	second week of life
Skin lesions	neutrophilic dermatosis, microthrombosis	neutrophilic dermatosis
Positive auto-antibodies	FANA, anti-β2 glycoprotein I, anti-thyroid, DAT	FANA, anti-β2 glycoprotein I, anti-thyroid
Thrombocytopenia	intermittent, mild	cyclic, moderate
Infections and microorganisms	viral pneumonias due to adenovirus, RSV, and *parainfluenza*; *Pneumocistis jiroveci* pneumonia; persistent norovirus diarrhea; multiple episodes of bacteremia (MRSA, K. pneumoniae, pseudomonas, gram-negative rods)	LRI due to rhinovirus, prolonged astrovirus diarrhea, recurrent Salmonella and *C. difficile* in stool, Salmonella bacteremia, pulmonary mycobacterial infection
Pulmonary nodules	yes	no
Seizures	no	yes
CD4/CD8 ratio	elevated	elevated
Immunoglobulin levels	elevated IgG, IgA, and IgE	elevated IgG, IgA, and IgE

Abbreviations are as follows: FANA, fluorescent anti-nuclear antibodies; DAT, direct anti-globulin test; RSV, respiratory syncytial virus; LRI, lower respiratory infection; MRSA, methicilin-resistant *Staphylococcus* aureus.

cells were counterstained with DAPI (all from ThermoFisher Scientific). Slides were mounted with ProLong Glass antifade reagent (ThermoFisher Scientific) and #1.5 glass coverslips (Corning) and cured for 24 hr before observation by confocal microscopy.

Imaging Acquisition

Fixed cells were imaged with a Zeiss Axio Observer Z.1 microscope stand equipped with a Yokogawa CSU10 spinning disk and a Hamamatsu Orca-R2 C10600 CCD camera. Laser lines included 405, 488, and 561 nm Coherent OBIS LX powered by a MultiLine LaserBank (Cairn Research). Emitted light was selected with the following filters as appropriate for the relevant dye: 460/50, 520/35, and 593/40 (Chroma Technology Corp). Imaging was performed with the plan apochromatic 63 × 1.4 NA oil-immersion objective, and MetaMorph software (v.7.8.13; Molecular Devices) was used for hardware control and image acquisition.

Analysis

Raw 3D stacks of images were exported for processing and analysis in Fiji[26] with a custom script. In brief, binary masks of individual cells were created with the threshold tool applied to the F-actin detection fluorescent channel. Cell outlines were filtered according to a size cutoff $> 10\ \mu m^2$. The fluorescence intensity of the BiP staining channel for each cell was then measured for the sum of all planes of the 3D stack within the cell outline mask and plotted with GraphPad Prism. For display purposes only, raw 3D stacks were reduced to a single plane with a maximum projection transformation and subjected to a linear scaling of their intensity, identically across all conditions, for optimal visualization.

Statistics

For IFN signature RT-qPCR, fold changes were calculated in relation to healthy donor cells. In total, three different healthy donors were used for determining the expression of type-1-IFN-induced genes. Representative figures of IFN signature results are presented as the mean ± SD of triplicate experiments. Mean fold-change values were compared to 1 with one-sample t tests (GraphPad Prism 7.0) to give an indication of differences between groups. For RT-qPCR quantification of ER stress markers, gene expression is presented as the relative ratio to GAPDH (mean ± SD). Imaging results were quantified with at least 20 cells per condition, and Student's t test (GraphPad Prism 7.0) was performed to compare means. Significance levels are expressed as follows: *$p < 0.05$, **$p < 0.01$, ***$p < 0.001$, ****$p < 0.0001$.

Results

Clinical Characterization of Individuals with *POMP*-Related Autoinflammation and Immune Dysregulation

We identified two unrelated individuals with a provisionally unique syndrome characterized by neonatal-onset autoinflammation, neutrophilic dermatosis, autoimmunity, and combined immune deficiency. The clinical manifestations at presentation were both unusual and overlapping (Table 1). Both presented during the first week of life with a perplexing constellation of papulo-erythematous skin lesions on the face, trunk, and extremities, and these progressed to necrotizing lesions and subsequent scarring (Figures 1 and S1). Biopsies of the lesions in both individuals revealed neutrophil infiltration and leukocytoclasis consistent with neutrophilic dermatosis. Biopsy specimens of individual A additionally confirmed a vasculitic rash showing thrombotic vasculopathy with vascular fibrinoid necrosis.

Initial immunologic evaluations of both individuals were characterized by consistent lymphocyte abnormalities (Tables 2, S2, and S3). In both, we observed high total T cell numbers with low $CD8^+$ T cell percentages and high $CD4^+$ percentages and counts, leading to an increased CD4/CD8 ratio. Interestingly, most $CD4^+$ T cells were skewed to a naive phenotype. B cell counts were initially extremely low; however, during the first year of life, some B cells were eventually detected, but they were unexpectedly heavily skewed toward a memory phenotype ($CD19^+CD27^+IgM^+IgD^-$ and $CD19^+CD27^+IgM^-IgD^-$).

Figure 1. Clinical Presentation of Two Unrelated Individuals Studied
(A) Persistent erythematous skin lesions with central ulceration in individual A have been present since the second week of life. Left to right: hand, index finger, face and nasal bridge, scalp, and diaper area.
(B) Persistent erythematous lesions with central ulceration in individual B. Left to right: foot, nasal bridge, face and scalp, and back and gluteal region.
(C) Histologic photomicrographs of skin lesions in individual A. Left: vasculopathic changes with fibrinoid endothelial necrosis of the vascular walls and extravasated erythrocytes, perivascular neutrophilic infiltrate, and karyorrhectic debris with focal dermal necrosis and edema and microthrombosis, suggestive of leukocytoclastic vasculitis as a component of a neutrophilic dermatosis or Sweet syndrome. Right: an interstitial dermatitis with histiocytic infiltrates, dermal edema, and red blood cell extravasation with perivascular neutrophils. Immunofluorescent stains were negative for IgA, IgM, IgG, fibrinogen C4, and C1q.
(D) Histologic photomicrographs of skin lesions from individual B. Left: epidermal spongiosis with superficial dermal neutrophilic infiltrates and karyorrhectic cellular debris predominantly in a perivascular distribution. Right: dermal perivascular neutrophilic infiltrate with karyorrhectic cellular debris and extravasated red cells suggesting a leukocytoclastic vasculitis in the context of neutrophilic dermatosis or Sweet's syndrome. Immunofluorescent stains for IgA, IgM, IgG, fibrinogen C4, and C1q were negative.

Circulating naive B cells ($CD19^+CD27^+IgM^+IgD^+$), which are typically common among B cells in infants, were not identified in either individual (Tables S2 and S3). Although the total number of peripheral B cells was low, both individuals had persistently high autoantibody titers with profiles resembling those found in systemic lupus erythematosus, including anti-nuclear antibodies (FANA) and anti-β2 glycoprotein I (anti-B2 GP I) autoantibodies (Tables 1 and S1). The high titers of anti-B2 GP I antibodies along with thrombotic skin lesions in individual A were consistent with anti-phospholipid syndrome.[27] Anti-B2 GP I antibodies included both IgG and IgA isotypes, and anti-thyroid autoantibodies included IgG, IgA, and IgM, suggesting that they were recently produced by these individuals' B cells and not passively acquired from their mothers, given that only IgG crosses the placenta. The mother of individual A was tested and did not have any of these autoantibodies. In consideration of their autoimmune phenotype, the presence of circulating plasmablasts was evaluated multiple times in individual B and once (before rituximab treatment) in individual A; both individuals showed increased circulating plasmablasts (Tables S2 and S3), consistent with their augmented autoantibody production. After this finding, individual A received rituximab, to which he showed a partial response.

Both individuals had numerous severe viral and bacterial infections. Individual A had several severe viral pneumonias due to adenovirus, respiratory syncytial virus, and parainfluenza virus; *Pneumocystis jiroveci* pneumonia; and prolonged norovirus gastrointestinal infection. Individual B had pneumonia due to rhinovirus, prolonged diarrhea due to astrovirus, *Salmonella* bacteremia, and pulmonary mycobacterial infection. Functional multiparametric flow-cytometry analyses showed impaired cytokine production in $CD8^+$ and $CD4^+$ T cells even when the effector T cell populations were exclusively assessed (Figures S2 and S3). The impaired cytokine production plausibly contributes to the infectious susceptibility in addition to the low percentage of $CD8^+$ T cells and low B cells. Thus, both individuals demonstrated objective and clinical findings consistent with combined

Table 2. Immunophenotype of Individuals Studied

	Individual A	Individual B	Normal Range
Lymphocyte Subsets	**Percentage (Absolute Count)**		
$CD3^+$ T cells	91% (5,562)	96% (9,303)	56%–84% (1,920–4,991)
$CD4^+$ T cells	87% (5,324)	89% (8,615)	41%–66% (1,546–3,673)
$CD8^+$ T cells	5% (306)	8% (775)	10%–28% (359–1,489)
CD4/CD8 ratio	17.3%	11.1%	1.67%–4.84%
$CD4RA^+$ naive CD4 T cells	82% (5,012)	86% (8,334)	3%–33% (134–969)
$CD4RO^+$ T cells	3% (183)	3% (291)	16%–42% (301–919)
$CD19^+$ B cells	5% (306)	0% (0)	6%–28% (256–1,579)
Memory B cells	0% (0)	0% (0)	1%–5% (19–131)
$CD56^+$ NK cells	5% (306)	3% (291)	6%–23% (137–478)
Regulatory T cells	0.6%	5%	NA
Immunoglobulins	**mg/dL**		
IgG	400–2,200[a]	320–2,200[a]	530–1,100
IgA	170–1,450	150–1,870	10–120
IgM	20–130	12–180	40–190
IgE	50–300	190–13,900	0–100

Lymphocyte subsets observed during the first evaluation of both individuals during their first month of life and immunoglobulin titer ranges observed during the first year of life (for further detail of lymphocyte subpopulations, refer to Tables S2 and S3).
[a]On IVIG supplementation.

immunodeficiency, autoimmunity, and autoinflammation. Given the severity of their clinical course, both individuals were ultimately referred for hematopoietic stem cell transplantation.

Heterozygous Frameshift Variants in the Penultimate Exon of *POMP* Escape NMD and Produce a Truncated Protein

A genetic cause for the disease trait was initially suspected on the basis of the early onset and severity of symptoms. Initial clinical sequencing of individual B did not identify a cause of immune dysregulatory disease. Research trio WES combined with bioinformatic analysis was performed to determine an underlying genetic contribution to the shared phenotype. In both probands, a heterozygous *de novo* frameshift variant in exon 5 of *POMP* (GenBank: NM_015932) was detected and confirmed by Sanger sequencing (Figures 2A and 2B). Individual A had a *de novo* c.342_348delinsACC (p.Phe114Leufs*18) (GenBank: NM_015932) frameshift variant, which is predicted to result in a truncated protein of 129 amino acids (~12 kDa) as a consequence of early termination in the −1 frame (Figure 2A). Individual B had a *de novo* c.334_335delAT (p.Ile112Trpfs*3) (GenBank: NM_015932) frameshift variant terminating in the −2 frame and predicted to result in a truncated protein product of 115 amino acids (~11 kDa) (Figure 2B). Both individuals were evaluated for additional variants in genes encoding proteasome subunits as well as PAC1–PAC4, and no known pathogenic or potentially damaging variants were identified in these genes.

Most RNA transcripts with premature termination codons (PTCs) undergo NMD.[28] NMD is a highly conserved mechanism that protects eukaryotes from truncated protein products that could cause disease by a dominant-negative or gain-of-function mechanism.[29] However, frameshift indels or missense substitutions that create a PTC shorter than 55 nucleotides upstream of the terminal exon-exon junction can give rise to mutant transcripts that are capable of escaping NMD.[28] These mutant transcripts are subsequently translated into aberrant truncated proteins that are potentially capable of causing disease (Figure 2C).

In both individuals, variants were located fewer than 50 nucleotides upstream of the last exon-exon junction. Therefore, we hypothesized that these variants could cause disease by escaping NMD and that a mutant PTC-containing mRNA could be translated into a prematurely terminated protein with potential dominant-negative or gain-of-function effects (Figure 2D). To evaluate this possibility, we sequenced cDNA samples derived from subject PBMCs, which revealed the presence of both wild-type and mutant transcripts, indicating that mutant mRNA had indeed escaped NMD (Figure 2E). These data are consistent with individual B's RNA sequencing results, which revealed 56 variant reads out of 196 total reads, also confirming that the transcript containing the variant allele escapes NMD. In addition, mutant and wild-type *POMP* mRNA

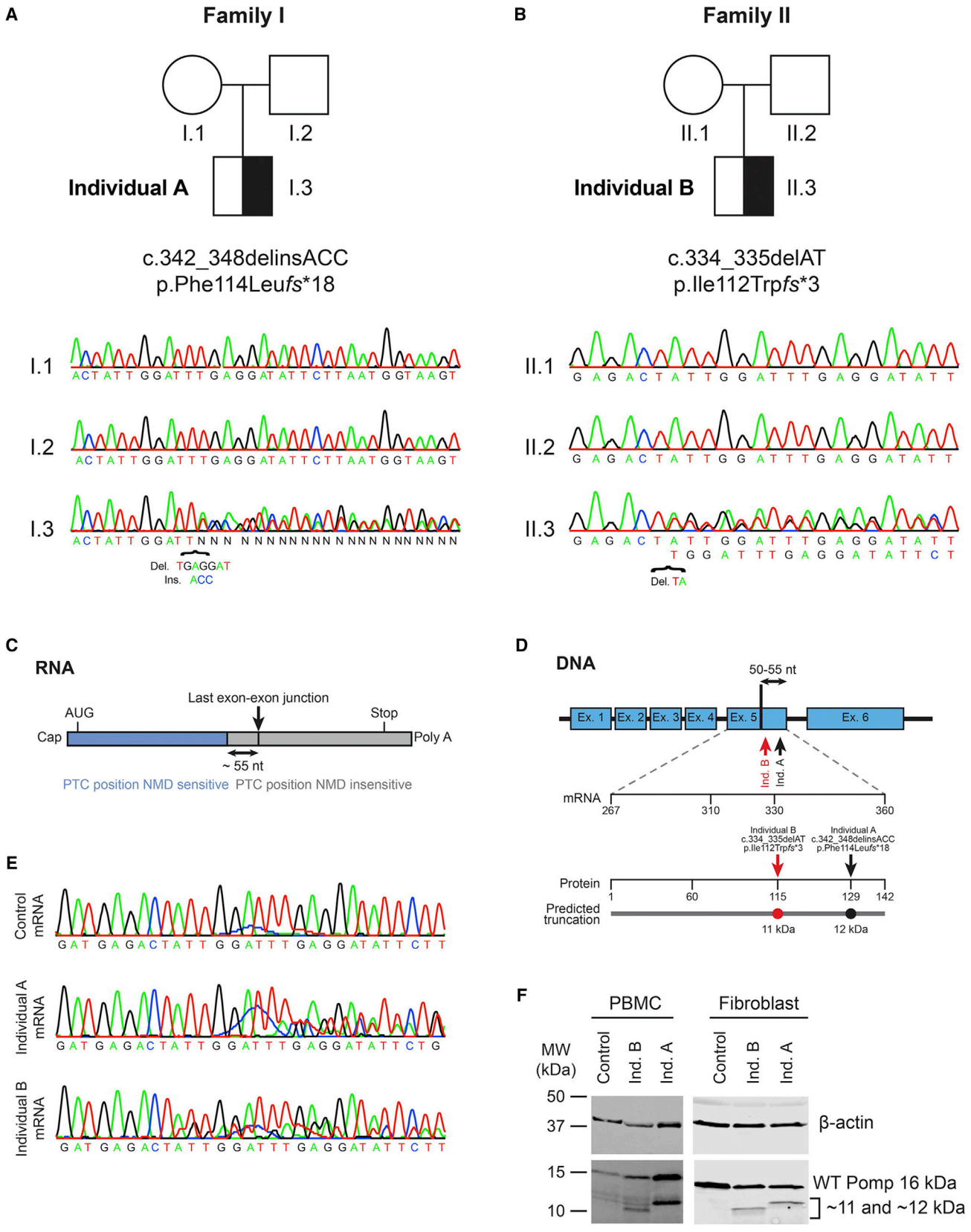

Figure 2. Truncating Frameshift *POMP* Variants Lead to mRNA Transcripts that Escape NMD and Result in a Truncated Protein
(A and B) *De novo POMP* variants identified in individuals A (A) and B (B). Half-filled boxes indicate heterozygous affected individuals A and B, and corresponding Sanger tracings are shown below.
(C) Diagram representing mRNA and the regions where PTCs will be sensitive or insensitive to undergoing NMD; a region approximately 50–55 nucleotides upstream of the last intron is susceptible to escaping NMD.

(legend continued on next page)

transcripts were quantified by RT-qPCR in PBMCs and cell lines, revealing consistent, at least partial NMD escape in both individuals (data not shown). To confirm the presence and anticipated relative molecular mass of an aberrant protein originating from this transcript, we performed western blot analyses by using subject-derived PBMCs, fibroblasts, and a B cell line from individual A. In all of these samples, we were able to consistently confirm the presence of a truncated protein at a predicted molecular weight of ~12 or ~11 kDa for individual A or B, respectively (Figure 2F). The identification of *POMP* variants and protein in two different tissue types (Figures 2F and S4) suggests heterozygosity rather than post-zygotic mosaicism or somatic mutation.

Mutant POMP Interferes with Proteasome Assembly

POMP serves as a chaperone for assembly of the standard proteasome and the immunoproteasome and is specifically required for the incorporation of the β subunits, including LMP7. We determined the impact of *POMP* variants in proteasome assembly by using SDS-PAGE and native gel overlays to evaluate the incorporation of proteasome subunits into the 20S and 26S proteasome. To perform these studies, we generated an EBV-transformed B cell line from individual A (verified to contain the variant allele). B cells from individual B could not be transformed despite multiple attempts. Using this cell line derived from individual A, we were able to demonstrate decreased incorporation of β1, β2, β5, LMP7, LMP2, and MECL1, as well as α2 and α6 subunits, whereas the incorporation of Rpn5 and Rpt6 from the 19S regulatory subunit was not perturbed (Figure 3A). In wild-type cells, the PA28-α subunit incorporates into the mature proteasome to catalyze protein degradation.[18] The cell line derived from individual A showed an increased amount of free proteasome activator PA28-α, indicating that this subunit was not being incorporated into a properly assembled proteasome and was most likely being upregulated to compensate for a dysfunctional proteasome (data not shown).

In order to test the impact of the variant in individual B, we used a fibroblast line derived from a skin biopsy from this individual. We established and utilized transformed fibroblast lines from both subjects to confirm a defect in proteasome assembly. Cells from both individuals showed decreased 20S proteasome quantities and increased proteasome precursor complexes stained with the α6 subunit (Figure 3B). For both individuals, Rpt6 quantities were not perturbed in fibroblasts lines, indicating proper assembly of the 19S proteasome (Figure 3C). We did not observe an accumulation of ubiquitinated products in SDS-soluble fractions of subject-derived cell lysates (Figure 3C). However, when analyzing SDS-insoluble fractions of cell lysates, we observed aggregation of ubiquitin-modified proteins in both individuals (Figure 3D), similar to what had been previously observed for CANDLE disease.[4] Thus, truncating *POMP* variants that escape NMD impair both standard proteasome and immunoproteasome assembly and result in the accumulation of ubiquitinated products in both individuals.

Defects in Proteasome Assembly Lead to Increased ER Stress and Activation of the Unfolded Protein Response, Causing a Type 1 IFN Inflammatory Response

Proteasome dysfunction can lead to increased endoplasmic reticulum (ER) stress, which activates the unfolded protein response (UPR) and the ER-membrane bound transcription factor TCF11/Nrf1.[30] The UPR is initiated through three ER transmembrane proteins: inositol requiring 1 (IRE1), which upregulates sXBP-1; PRK-like ER kinase (PERK), which phosphorylates eIF2α (peIF2α); and activating transcription factor 6 (ATF6).[31] An ER chaperone and ER stress sensor, immunoglobulin binding protein (BiP) is bound to these ER membrane sensors and dissociates from them to activate the UPR. Interestingly, a liver biopsy from individual B was available and showed enlarged ER, suggesting increased ER stress (Figure S1). To evaluate ER stress in subject cells, we performed RT-qPCR of PBMC cDNA samples and identified increased ATF6, BiP, and sXBP1 transcripts in individual B, whereas only sXBP1 was increased in individual A (Figure 4A). Importantly, at the time these samples were obtained from individual A, he had received considerable immunosuppression. At the protein level, the B cell line of individual A did not show a significant increase in either the amount of UPR-related protein GADD34 or the amount of transcription factor TCF11/Nrf1 (Figure 4B). It also failed to express the phosphorylated form of eIF2α (peIF2α) at the expected size of 37 kDa. However, when ER stress markers were assessed in this cell line by more sensitive RT-qPCR methods, cells derived from individual A demonstrated a clear upregulation of the UPR (Figure 4C), as evidenced by increased quantities of ATF6, BiP, and sXBP1. Fibroblast lines derived from both individuals contained increased amounts of peIF2α, which was more evident in individual B, in whom increased amounts of TCF11/Nrf1 were also detected (Figure 4B). The quantity of GADD34 remained unaffected by the presence of either of the *POMP* variants in these cells, suggesting that the PERK pathway might be

(D) Diagram representing *POMP* DNA, *POMP* mRNA, and POMP maps subject variants fewer than 55 nucleotides upstream of the last exon-exon junction and to the C-terminal region of POMP. Red and black arrows indicate the predicted localization of early stop codons at the protein level; red and black dots indicate the corresponding predicted molecular weights of truncated proteins.
(E) Sanger tracing of cDNA obtained from subject PBMCs shows the presence of both wild-type and mutant transcripts for both individuals. Additionally, primers including intronic sequence of genomic *POMP* failed to amplify *POMP* from cDNA, ruling out genomic DNA contamination (not shown).
(F) Western blot probing for POMP in lysates obtained from subject-derived PBMCs and fibroblasts lines. These images are representative of at least three separate western blots performed for each sample.

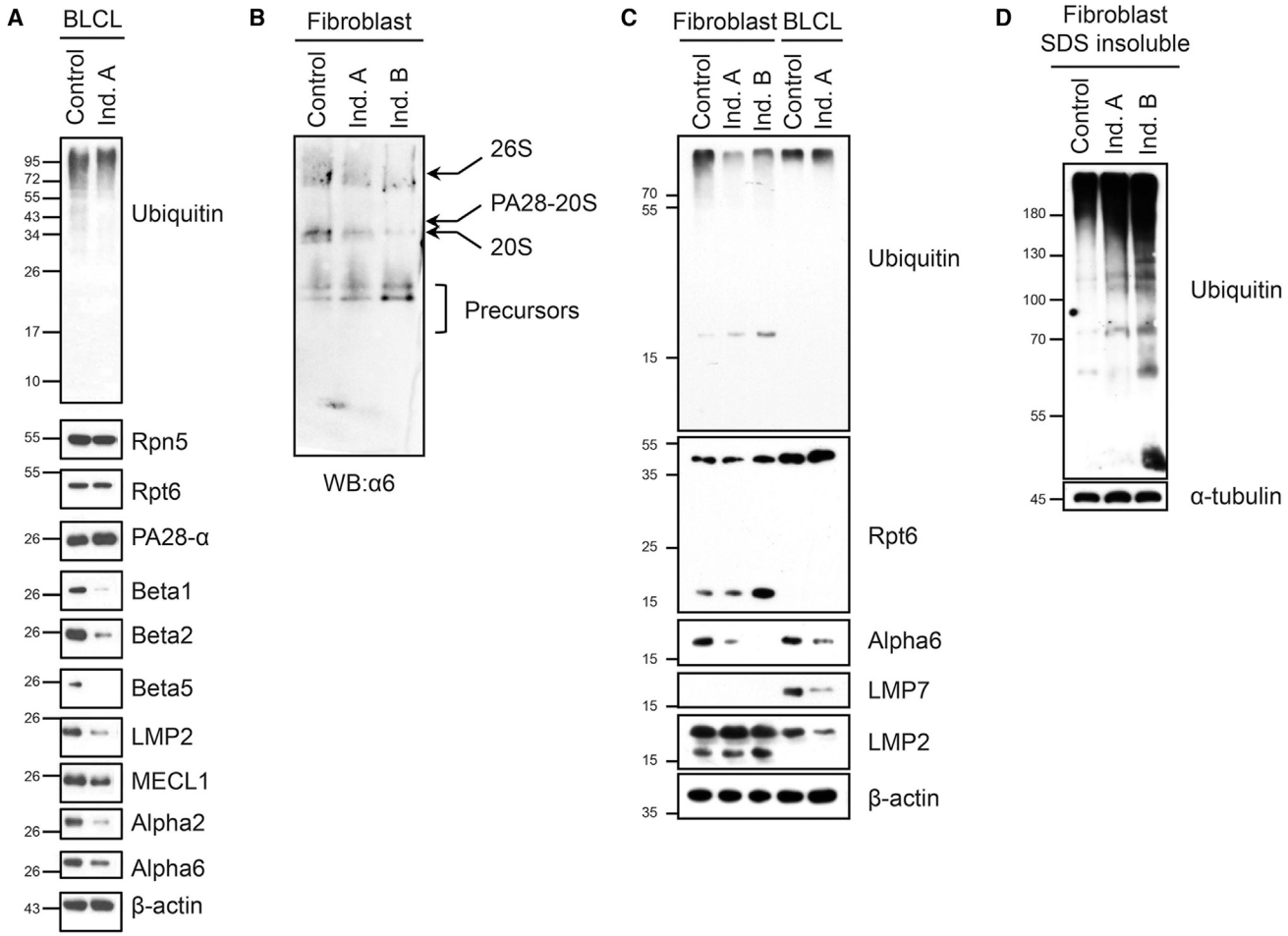

Figure 3. *POMP* Variants Interfere with Proteasome Assembly

(A) SDS-PAGE performed in an EBV-transformed B cell line (BLCL) from individual A shows decreased incorporation of Beta1, Beta2, Beta5, and LMP7 subunits as well as decreased incorporation of Alpha2 and Alpha6 in comparison with control cells. No accumulation of ubiquitinated products was observed in SDS-soluble fractions. β-actin was used as a loading control.

(B) Non-denaturing (native) gels with proteasome bands visualized with anti-α6 antibody show decreased 20S and 26S proteasomes in fibroblast samples from both individuals compared with control cells.

(C) SDS-PAGE of a subject-derived BLCL and transformed (SV40) fibroblast lines probed for proteasome subunits shows decreased incorporation of Alpha6 in both individuals and decreased incorporation of Alpha 6, LMP7, and LMP2 in the BLCL from individual A in the last lane in comparison with control fibroblasts and B cells lines, respectively. β-actin was used as a loading control.

(D) Gel probing for ubiquitinated products in SDS-insoluble fractions of transformed (SV40) fibroblast lines shows increased accumulation of ubiquitin-protein conjugates in both individuals compared with a control fibroblast line. Anti-α-tubulin antibody was used as a loading control.

Images are representative of three individual repeats.

predominantly initiated in cells expressing *POMP* variant B. RT-qPCR assessment of ER stress markers in fibroblast lines showed increased amounts of ATF6 and BiP in both individuals, whereas sXBP1 was only significantly upregulated in individual B (Figure 4C). Together, these data indicate that there is increased ER stress and a clear activation of the UPR in both individuals, albeit to a lesser extent in individual A.

Transcriptional studies performed in individuals with CANDLE disease and biallelic mutations in *PSMB4* or *PSMB8* have shown increased expression of type-1-IFN-inducible genes.[4] The genes that were most upregulated in these individuals were, in decreasing order of magnitude, *IFI27*, *RSAD2*, *USP18*, *IFI44L*, *IFIT1*, *OAS1*, *IFI44*, *ISG15*, *OAS3*, and *MX1*. Given the clinical phenotype of the individuals described in this work, the impact of the *POMP* variants in proteasome assembly, and the increased ER stress, we speculated that their cells would demonstrate increased expression of type-1-IFN-inducible genes, or an "IFN signature," similar to that observed in individuals with CANDLE disease and mutations affecting proteasome subunits. To establish *POMP*-related autoinflammation and immune dysregulation (PRAID) as an interferonopathy, we evaluated the expression of type-1-IFN-inducible genes by RT-qPCR in PBMCs. In both individuals, the expression of type 1 IFN signature genes was at least 4-fold higher than in healthy control PBMCs (Figure 4D). Similar trends were identified in the EBV-transformed B

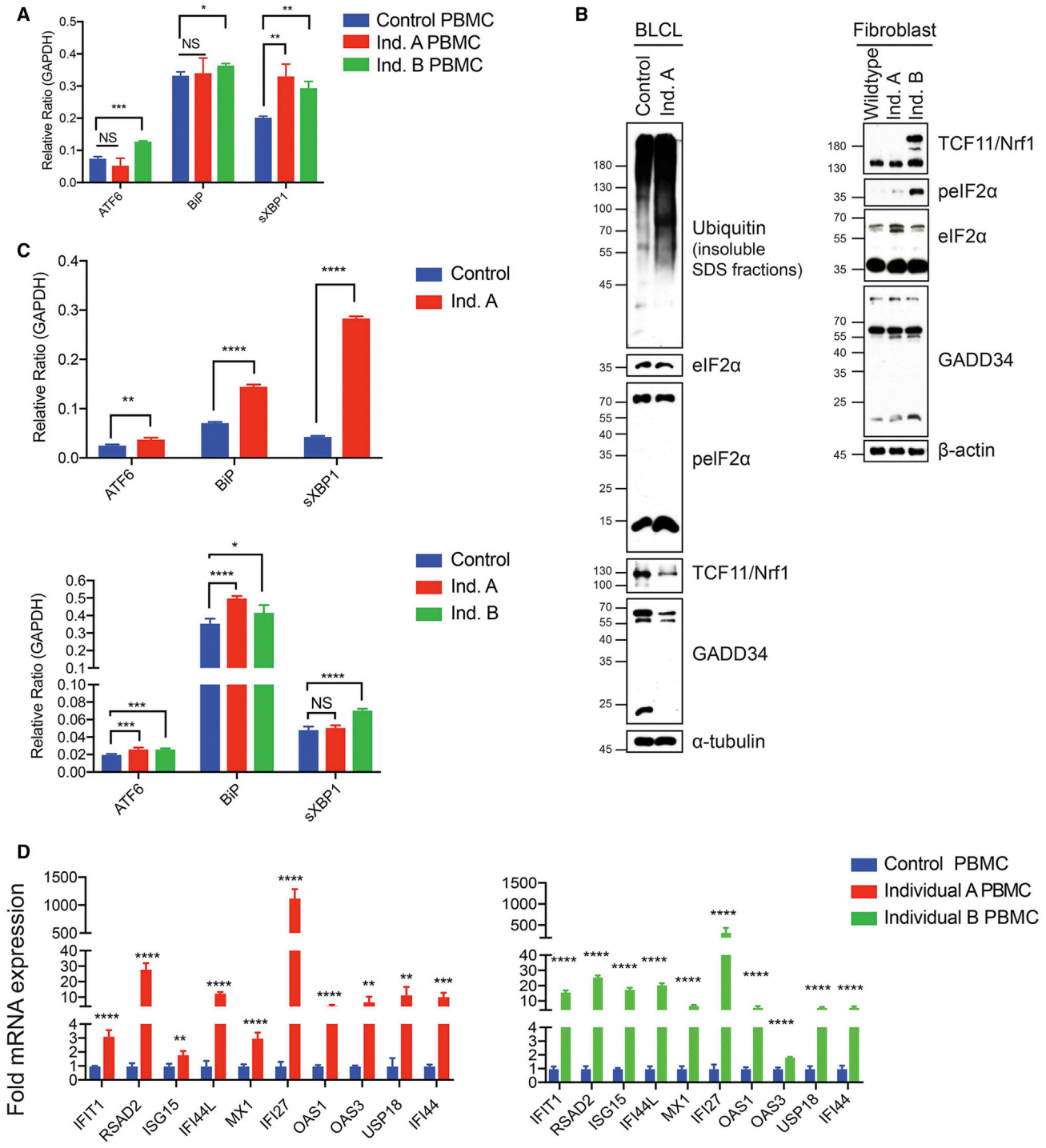

Figure 4. Proteasome Dysfunction Leads to ER Stress and Type 1 IFN Signature

(A) ER stress (BiP) and UPR markers ATF6 and sXBP1were quantified by RT-qPCR in PBMCs.

(B) Western blot analysis of a BLCL and fibroblast lines probed for the UPR markers eIF2α, peIF2α, and GADD34 as well as for the ER-membrane-bound transcription factor TCF11/Nrf1. Equal protein loading was ensured by membrane probing with anti-α-tubulin and anti-β-actin antibodies.

(C) Quantification of ER stress markers by RT-qPCR in fibroblast cell lines from both individuals and a B cell line from individual A.

(D) mRNA expression of IFN signature genes in PBMC-derived cDNA was measured by RT-qPCR and is expressed in relation to (normalized to) expression of control PBMC samples. Data are representative of three independent biological experiments performed in quadruplicate; bars represent mean ± SD of four replicates. mRNA expression was compared with that of control PBMC samples by Student's t test. All differences shown were also statistically significant in each of the independent biological repeats using at least two different control PBMC samples.

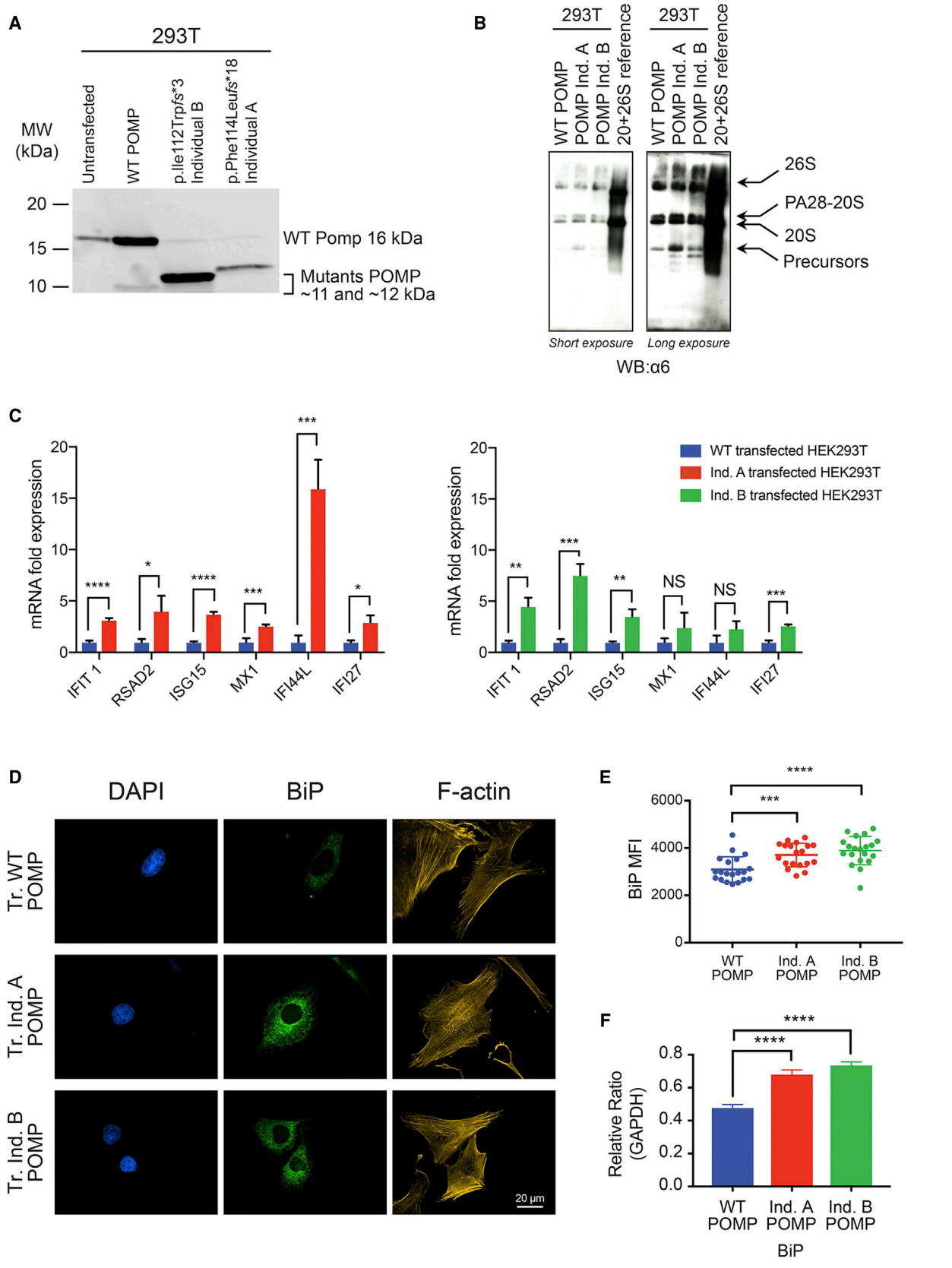

Figure 5. Overexpression of Mutant POMP in HEK293T Cells and Control Fibroblast Cell Lines Recapitulates PRAID Cellular Phenotype, Suggesting a Dominant-Negative Mechanism

(A) Western blot probing for POMP shows efficient transfection of HEK293T cell lines 24 hr after transfection.

(legend continued on next page)

cell line from individual A (Figure S4D) and fibroblast lines from both individuals (data not shown), indicating that truncating *POMP* variants that escape NMD lead to a type 1 IFN signature in both hematopoietic and non-hematopoietic cells.

POMP Variants Lead to an Increased IFN Signature by a Dominant-Negative Mechanism

We hypothesized that only *POMP* variants capable of escaping NMD would cause PRAID. Interestingly, when comparing the location of our variants with the two previously reported variants without mechanistic details,[4,8] we noted that both prior individuals carried heterozygous *POMP* frameshift variants in the same unique region predicted to escape NMD (c.334_335delAT [p.Ile112Trpfs*3] [GenBank: NG 027550.1] and c.344_345insTTTGA [p.Glu115Aspfs*20] [GenBank: NM_015932]). Furthermore, the individual described originally by Gatz et al.[8] had the same *POMP* variant as our individual B but carried an additional *MCM3AP* (MIM: 603294) variant that was thought to also contribute to his phenotype. Thus, PRAID is characterized by a CANDLE-like syndrome with an increased IFN signature or "interferonopathy" caused exclusively by truncating *POMP* variants that escape NMD.

In order to evaluate the exclusivity of PRAID and NMD-escaping *POMP* variants more broadly, we further examined the genetic mechanism by which such variants cause disease. Bioinformatically, the absence of loss-of-function variants in *POMP* in the ExAC Browser (~121,000 alleles) suggests that heterozygous loss of function does not occur frequently in healthy individuals. In addition, the clustering of *POMP* variants within the penultimate exon in our two individuals and the two previously described individuals, combined with the observation that no other *POMP* frameshifts are known to occur in humans, argues in favor of a dominant-negative mechanism rather than mere haploinsufficiency. Furthermore, previous evidence suggesting POMP dimerization and tetramerization[11] provides a suitable background for a dominant-negative mechanism in which an aberrant truncated protein could impair protein multimerization and therefore result in a phenotype that is more severe than haploinsufficiency.

To investigate this hypothesis, we overexpressed mutant, truncated POMP representing the variants identified in individuals A and B in a HEK293T cell line expressing wild-type POMP endogenously. Mutant or wild-type *POMP* constructs were transfected into HEK293T cells, and successful transfection was confirmed by western blots in which both endogenous wild-type and transfected wild-type or mutant POMP was detectable (Figure 5A). HEK293T cell lines transiently transfected with mutant *POMP* did not show substantial differences in the 20S and 26S proteasome amounts (Figure 5B). This is an expected result given the stability of the HEK293T endogenous proteasome complexes (5 days) and the short transfection time used (24 hr). Importantly, however, our native-PAGE analysis showed that the proteasome assembly process was impaired in cells expressing either one of the two *POMP* variants but not in their wild-type counterparts. This was evidenced by the accumulation of proteasome precursors in cells expressing these two variants, as determined by western blotting using an antibody specific to the alpha6 subunit (Figure 5B). The expression of type-1-IFN-inducible genes was measured by RT-qPCR 24 hr after transient transfection. HEK293T cells transfected with the mutant *POMP* constructs showed increased expression of type-1-IFN-induced genes, indicating a disease-promoting toxic dominant-negative effect of the truncated protein and resembling the biological phenotype of both individuals studied (Figure 5C).

To further confirm that increased ER stress observed in these individuals' cells was also derived from a dominant-negative mechanism, we stably transduced control fibroblasts with each of the mutants and quantified BiP by confocal microscopy and RT-qPCR. As expected, the amounts of the ER stress marker BiP were significantly higher in fibroblasts stably transduced with either of the mutant *POMP* constructs than in those transduced with wild-type *POMP* (Figures 5D–5F). Thus, bioinformatics, biochemical evaluations of proteasome assembly, quantification of ER stress, and IFN signatures demonstrate that truncating *POMP* variants lead to PRAID most likely through a dominant-negative mechanism.

Discussion

NMD is a highly conserved mechanism for protecting species from the toxic effects of truncated proteins. Transcripts encoding early termination codons are degraded to preferably result in haploinsufficiency and avoid a more deleterious dominant-negative or gain-of-function disease. Transcript susceptibility to NMD can substantially modify the severity and clinical phenotype of genetic diseases.[32] In the case of truncating mutations for which the gene product has maintained some residual function,

(B) Native-PAGE analysis of proteasomes in transiently transfected HEK293T cell lines shows the accumulation of proteasome precursors in cell lines transfected with both *POMP* mutants.
(C) Expression of IFN signature genes was measured by RT-qPCR in a transfected HEK293T cell line and determined 24 hr after transient transfection gene expression was compared between HEK293T cells transfected with mutants (red or green) and those transfected with wild-type constructs (blue). Western blots and RT-qPCR results are representative of at least three independent biological repeats.
(D) Confocal microscopy images of control fibroblasts stably transduced with wild-type and either *POMP* mutant. Staining for DAPI (blue), BiP (green), and phalloidin were used to identify filamentous actin (yellow).
(E) Imaging quantification of BiP MFI within 3D z stacks per individual cell; 20 cells were analyzed per condition (n = 20).
(F) RT-qPCR quantification of BiP in fibroblasts stably transduced with either wild-type or mutant *POMP* constructs.

NMD of the mutant transcript can exacerbate the phenotype through conversion of a hypomorphic allele to a loss-of-function allele. Such is the case for *SOX10*, where individuals with truncating variants that escape NMD exhibit a milder phenotype.[33,34] In contrast, in situations in which a truncated protein product would otherwise lead to a dominant-negative or gain-of-function mechanism, effective NMD can ameliorate the clinical phenotype.[32] When variants lead to the transcription of mRNA bearing a PTC within the last 55 nucleotides of the terminal exon-exon junction, these transcripts are susceptible to escaping this protective mechanism. To date, only a handful of genetic syndromes where the disease mechanism necessitates that mutant transcripts escape NMD have been described. Notable examples include AD Robinow syndrome types 2 (MIM: 616331; associated with *DVL1* [MIM: 601365]) and 3 (MIM: 616894; associated with *DVL3* [MIM: 601368]), brachydactyly type B (MIM: 113000; associated with *ROR2* [MIM: 602337]), Gibbs syndrome (MIM: 615829; associated with *AHDC1* [MIM: 615790]), gingival fibromatosis (MIM:617626; associated with *REST* [MIM: 600571]), intellectual developmental disorder with gastrointestinal difficulties and high pain threshold (MIM: 617450; associated with truncating variants in *PPM1D* [MIM: 605100]), and AD Meier-Gorlin syndrome (MIM: 616835; associated with *GMNN* [MIM: 602842]).[35–40]

For primary immunodeficiencies, more than 300 genetic causes have been identified, and the vast majority are recessive. Only about 40 AD PID-associated genes have been described, and most of the associated diseases result from haploinsufficiency. Within AD PIDs, approximately 17 are caused by either a gain-of-function or dominant-negative mechanism, and these conditions are clustered in individuals with autoinflammatory or autoimmune phenotypes;[1,41] however, none require NMD escape. PRAID is an immune dysregulation disease in which NMD escape has been identified as the disease-causing mechanism. Consistent with this interpretation, the two previously reported individuals with *POMP* variants and a similar phenotype carry heterozygous frameshift variants mapping to the same genic region predicted to escape NMD.[4,8] Although those prior reports did not evaluate NMD or the biological mechanism by which variation in *POMP* contributes to disease in subject-derived cells, the four individuals together with biological evidence presented here make a case for PRAID as an immune disease of NMD escape. Future work should more exactly evaluate this by using previously identified methods such as NMD reporters or NMD knockdown in order to learn more about both this disease and NMD in general.[34,42]

Many bioinformatic algorithms assume that heterozygous frameshift variants or early termination codons result in haploinsufficiency. When these variants escape NMD, the mechanism is more likely to be dominant negative or gain of function, and additional investigation is warranted. It is important to emphasize that the location of the frameshift variant does not necessarily predict the location of the PTC, given that occasionally dozens or even hundreds of aberrant amino acids will be translated before the termination codon in the abnormal reading frame. The development of new algorithms to detect these types of variants could help identify novel AD diseases. Indeed, an algorithm designed to identify potentially pathogenic variant alleles that escape NMD when applied to a database of around 6,000 exomes from subjects with suspected Mendelian disease genes independently identified *POMP* as a candidate gene (Z.H.C-A. et al., unpublished data).

Homozygous loss-of-function variants (homozygous variants predicted to undergo NMD or homozygous deletions) in *POMP* are not present in public databases and have not been identified in humans. Furthermore, a *Pomp*-deficient mouse has not been described, and it remains unclear whether it would be viable. To our knowledge, the only proteasome chaperone knockout model that has been studied is for PAC1, and these mice die during embryonic development.[43] According to public databases (DECIPHER and gnomAD), heterozygous deletions and early frameshifts in *POMP* have been found in individuals with phenotypes that do not overlap PRAID and also in healthy individuals, suggesting that haploinsufficiency is unlikely. Previous reports suggest that POMP organizes proteasome assembly at the ER.[14] Structural studies with yeast proteasome precursor complexes suggest that the yeast POMP homolog Ump1 facilitates proteasome assembly as a dimer.[44] Mutations in genes whose products oligomerize, multimerize, or form part of protein complexes to perform their function can result in phenotypes that are more severe than haploinsufficiency through a dominant-negative mechanism. Truncating *POMP* mutations that escape NMD are unlikely to result in complete loss of function; rather, the mutant protein could perturb a majority of the POMP dimers, resulting in a phenotype that appears more severe than haploinsufficiency alone. In this context, the mutated product (POMP monomer) could interfere with the activity of the wild-type product, namely assisting proteasome assembly, by interfering with complex or multimer formation[45,46] and thus "poisoning" the function of the wild-type product. The phenotypic findings in both individuals—confirmation of a defect in proteasome assembly, increased ER stress, and increased expression of type-1-IFN-induced gene—suggest a proteasome functional deficiency akin to that of individuals with CANDLE syndrome and AR variants in proteasome subunits. Similar to cells from individuals with CANDLE,[47] the fibroblast line from individual B showed higher amounts of TCF11/Nrf1, the transcription factor for proteasome genes, than control cells, thereby supporting the notion that proteasomes are not fully functional in these cells. Furthermore, transfection of mutants induced the accumulation of proteasome precursors, leading to increased expression of type-1-IFN-regulated genes and augmented ER stress in comparison with cell lines endogenously expressing POMP (transfected with WT *POMP*

constructs), demonstrating a proof of concept of the linkage between the presence of the truncated POMP in the face of wild-type protein and an immunological phenotype. The transfection experiments also remove the biological mechanism from any other background genetic modifiers that could theoretically be active in these individuals. On the basis of bioinformatic predictions and our collective data, there are strong indications that PRAID is caused by a dominant-negative mechanism. As an additional consideration, endogenous micro-RNA-101 has been shown to target the 3′ UTR of *POMP* mRNA to downregulate protein quantities,[48] and alterations in the 3′ UTR of mutant transcripts could potentially also contribute to a dominant-negative effect.

Notably, both individuals had a remarkably similar presentation of their illness, and both histologic and immunologic findings were almost identical. Individual A had a more severe course in terms of infection and immune dysregulation. Differences in susceptibility to NMD could account for this difference, but the proportion of mutant to wild-type POMP in western blots of PBMCs and fibroblasts from both individuals did not differ significantly, arguing that the mRNA and protein stabilities of the two mutant POMP proteins are similar (data not shown). The degree to which differential aberrancy of mutant POMP can contribute to the severity of the phenotype is not known, but our transfection experiments suggest that these mutants would have a similar biologic effect. Thus, other factors such as infections, treatments, or variants in modifying genes could contribute to the greater severity of the phenotype in individual A. Future recognition and study of other individuals with PRAID will help answer these questions.

The individuals described in this work share some phenotypic features with CANDLE syndrome, but other characteristics are unique to both individuals described here and differ from individuals with CANDLE syndrome both clinically and immunologically. First, individuals A and B presented with neutrophilic dermatosis that was unresponsive to steroid treatment during the first 2 weeks of life. Although chronic neutrophilic dermatosis is characteristic of CANDLE, neonatal onset is not described as a consistent feature of neutrophilic dermatosis in CANDLE syndrome. Neonatal-onset neutrophilic dermatosis, or neonatal Sweet's syndrome, should prompt evaluation for PRAID. Second, unlike individuals with CANDLE, the two individuals reported here did not show aseptic fever; they presented with fever only during confirmed infectious episodes. Another distinguishing feature is the absence of lipodystrophy or abdominal fat deposition in individuals with PRAID through approximately 3 years of follow up. It remains possible, however, that lipodystrophy could develop at a later age. Finally, in terms of immune phenotype, both individuals with truncating *POMP* variants have elevated $CD4^+/CD8^+$ T cell ratios with predominantly naive T cells, similar to what has been described in individuals with mutations in proteasome subunits and $Mecl1^{-/-}$ mice. Decreased incorporation of LMP7 and MECL1 into the proteasome could account for low $CD8^+$ T cell counts in these individuals with *POMP* variants. Most importantly, both individuals described here share a remarkably severe immunodeficient phenotype characterized by recurrent viral and bacterial infections, including disseminated mycobacterial disease in individual B and severe recurrent viral infections and *Pneumocystis jiroveci* in individual A. Furthermore, both required frequent and prolonged hospitalizations for systemic viral and bacterial infections despite immunoglobulin prophylaxis, indicating that the infectious susceptibility is most likely secondary to T cell dysfunction. This has led both of these individuals to be referred for hematopoietic stem cell transplantation. Although infections have been described as part of the clinical spectrum in CANDLE, severe infections do not represent a prominent feature despite their low $CD8^+$ T cell numbers. We believe that this difference could be explained by the remarkably similar reduction in T cell cytokine production upon TCR stimulation in both individuals.

The immunoproteasome plays an important role in cytokine production. Selective LMP7 inhibition with PR-957 reduces the production of TNF-α, IL-23, IL-6, IFN-γ, and IL-2 in human T cells.[49] Interestingly, neither $Lmp7^{-/-}$ nor $LMP7^{-/-}Mecl1^{-/-}$ mice have a defect in T cell cytokine production. It has been proposed that this occurs because these deficient mice are able to compensate by incorporating the constitutive β5 subunit into the i20S to facilitate cytokine production.[50] Bearing in mind the critical role of POMP for β5 and LMP7 incorporation into the 20S and i20S proteasomes, respectively, it seems plausible that upon infection, PRAID-affected individuals are unable to compensate and consequently exhibit the observed defect in T cell cytokine production underlying their combined immunodeficient phenotype, in addition to a reduced $CD8^+$ T cell number. In agreement with our observations, the individual described by Gatz et al. also presented with severe opportunistic infections, including *Pneumocystis jiroveci* pneumonia and systemic atypical mycobacterial infection by *Mycobacterium avium*.[8] Our observations suggest that this severe T cell defect could be unique to PRAID compared with other forms of PRAAS. Interestingly, the B cell phenotype of the individuals described here also differs substantially from the phenotype present in CANDLE syndrome. Although B cells in CANDLE consist mostly of a naive phenotype ($CD19^+CD27^-$), individuals A and B initially lacked B cells but later developed B cells with a switched memory phenotype ($CD19^+CD27^+IgM^+IgD^-$ or $CD19^+CD27^+IgM^-IgD^-$). This suggests that a limited number of aberrant B cells were able to mature and expand, which would be consistent with the autoimmunity and autoantibodies found in individuals A and B. Future work is needed to investigate the mechanism by which defects specifically in POMP lead to this remarkable phenotypic B cell skewing. We consider PRAID a distinct interferonopathy associated with profound combined immunodeficiency within the larger spectrum of PRAAS.

The exact mechanism leading to abnormal IFN transcription in PRAAS remains largely unknown. Individuals with CANDLE syndrome accumulate ubiquitinated products that are not degraded by the proteasome, and this process is believed to contribute to the development of a type 1 IFN gene signature.[4] Throughout this work, we have confirmed that PRAID is an interferonopathy. Immunoproteasomes are required for efficient degradation of polyubiquitinated proteins, and POMP knockdown results in an accumulation of these proteins that have been tagged for proteasomal degradation.[20,48] Similar to individuals with CANDLE, individuals with PRAID show aggregation of ubiquitinated proteins in the SDS-insoluble fractions, presumably leading to ER stress and contributing to an increased type-1-IFN-induced gene expression, as demonstrated by our experiments in subject cells and healthy cell lines transfected with *POMP* mutants.

In conclusion, we define PRAID in two unrelated individuals as being characterized by neonatal-onset immune dysregulation and combined immunodeficiency caused by truncating variants in *POMP*, whereby transcripts that escape NMD result in a truncated protein that leads to a dominant-negative (i.e., antimorphic) allele. PRAID is therefore an inherent immunological defect mechanistically characterized by NMD escape.

Supplemental Data

Supplemental Data include a description of primers used for RT-qPCR, four figures, and two tables and can be found with this article online at https://doi.org/10.1016/j.ajhg.2018.04.010.

Consortia

Members of the Undiagnosed Diseases Network include David R. Adams, Mercedes E. Alejandro, Patrick Allard, Euan A. Ashley, Mahshid S. Azamian, Carlos A. Bacino, Ashok Balasubramanyam, Hayk Barseghyan, Gabriel F. Batzli, Alan H. Beggs, Babak Behnam, Hugo J. Bellen, Jonathan A. Bernstein, Anna Bican, David P. Bick, Camille L. Birch, Devon Bonner, Braden E. Boone, Bret L. Bostwick, Lauren C. Briere, Donna M. Brown, Matthew Brush, Elizabeth A. Burke, Lindsay C. Burrage, Manish J. Butte, Shan Chen, Gary D. Clark, Terra R. Coakley, Joy D. Cogan, Cynthia M. Cooper, Heidi Cope, William J. Craigen, Precilla D'Souza, Mariska Davids, Jean M. Davidson, Jyoti G. Dayal, Esteban C. Dell'Angelica, Shweta U. Dhar, Katrina M. Dipple, Laurel A. Donnell-Fink, Naghmeh Dorrani, Daniel C. Dorset, Emilie D. Douine, David D. Draper, Annika M. Dries, David J. Eckstein, Lisa T. Emrick, Christine M. Eng, Gregory M. Enns, Ascia Eskin, Cecilia Esteves, Tyra Estwick, Liliana Fernandez, Carlos Ferreira, Paul G. Fisher, Brent L. Fogel, Noah D. Friedman, William A. Gahl, Emily Glanton, Rena A. Godfrey, David B. Goldstein, Sarah E. Gould, Jean-Philippe F. Gourdine, Catherine A. Groden, Andrea L. Gropman, Melissa Haendel, Rizwan Hamid, Neil A. Hanchard, Lori H. Handley, Matthew R. Herzog, Ingrid A. Holm, Jason Hom, Ellen M. Howerton, Yong Huang, Howard J. Jacob, Mahim Jain, Yong-hui Jiang, Jean M. Johnston, Angela L. Jones, David M. Koeller, Isaac S. Kohane, Jennefer N. Kohler, Donna M. Krasnewich, Elizabeth L. Krieg, Joel B. Krier, Jennifer E. Kyle, Seema R. Lalani, C. Christopher Lau, Jozef Lazar, Brendan H. Lee, Hane Lee, Shawn E. Levy, Richard A. Lewis, Sharyn A. Lincoln, Sandra K. Loo, Joseph Loscalzo, Richard L. Maas, Ellen F. Macnamara, Calum A. MacRae, Valerie V. Maduro, Marta M. Majcherska, May Christine V. Malicdan, Laura A. Mamounas, Teri A. Manolio, Thomas C. Markello, Ronit Marom, Martin G. Martin, Julian A. Martínez-Agosto, Shruti Marwaha, Thomas May, Allyn McConkie-Rosell, Colleen E. McCormack, Alexa T. McCray, Jason D. Merker, Thomas O. Metz, Matthew Might, Paolo M. Moretti, Marie Morimoto, John J. Mulvihill, Jennifer L. Murphy, Donna M. Muzny, Michele E. Nehrebecky, Stan F. Nelson, J. Scott Newberry, John H. Newman, Sarah K. Nicholas, Donna Novacic, Jordan S. Orange, J. Carl Pallais, Christina G.S. Palmer, Jeanette C. Papp, Neil H. Parker, Loren D.M. Pena, John A. Phillips III, Jennifer E. Posey, John H. Postlethwait, Lorraine Potocki, Barbara N. Pusey, Chloe M. Reuter, Amy K. Robertson, Lance H. Rodan, Jill A. Rosenfeld, Jacinda B. Sampson, Susan L. Samson, Kelly Schoch, Molly C. Schroeder, Daryl A. Scott, Prashant Sharma, Vandana Shashi, Edwin K. Silverman, Janet S. Sinsheimer, Kevin S. Smith, Rebecca C. Spillmann, Kimberly Splinter, Joan M. Stoler, Nicholas Stong, Jennifer A. Sullivan, David A. Sweetser, Cynthia J. Tifft, Camilo Toro, Alyssa A. Tran, Tiina K. Urv, Zaheer M. Valivullah, Eric Vilain, Tiphanie P. Vogel, Daryl M. Waggott, Colleen E. Wahl, Nicole M. Walley, Chris A. Walsh, Jijun Wan, Michael F. Wangler, Patricia A. Ward, Katrina M. Waters, Bobbie-Jo M. Webb-Robertson, Monte Westerfield, Matthew T. Wheeler, Anastasia L. Wise, Lynne A. Wolfe, Elizabeth A. Worthey, Shinya Yamamoto, Yaping Yang, Amanda J. Yoon, Guoyun Yu, Diane B. Zastrow, Chunli Zhao, and Allison Zheng.

Conflicts of Interest

J.R.L. has stock ownership in 23andMe, is a paid consultant for Regeneron Pharmaceuticals, has stock options in Lasergen Inc., and is a co-inventor on multiple United States and European patents related to molecular diagnostics for inherited neuropathies, eye diseases, and bacterial genomic fingerprinting. The Department of Molecular and Human Genetics at Baylor College of Medicine derives revenue from molecular genetic testing offered in the Baylor-Genetics Laboratories (http://www.bcm.edu/geneticlabs/).

Acknowledgments

We acknowledge members of the Undiagnosed Diseases Network (listed in the Consortia section) for their participation in this study. We are also grateful to Lisa Bouchier-Hayes for her scientific advice and to the following clinical consult physicians who participated in patient care: Ryan Himes, gastroenterology; Timothy Vece, pulmonology; Carl Allen and Caridad Martinez, hematology; Reagan Hunt, dermatology; and Alisa Acosta, nephrology. Finally, we thank both individuals described in this manuscript and their families for facilitating this work. Research reported in this manuscript was supported in part by the NIH National Institute of Allergy and Infectious Diseases (R01AI120989 to J.S.O.), the Jeffrey Modell Foundation (to J.S.O.), the NIH National Institute of Neurological Disorders and Stroke (R35NS105078 to J.R.L.), the National Human Genome Research Institute and National Heart, Lung, and Blood Institute (U01 HG006542 to the Baylor Hopkins Center for Mendelian Genomics), the Fritz-Thyssen-Foundation (AZ:10.16.2.022 MN to E.K.), the German Research Foundation (SFBTRR 167 A04 to E.K.), and the NIH Common Fund through the Office of Strategic Coordination and Office of the NIH Director (U01 HG007709). The content is solely the

responsibility of the authors and does not necessarily represent the official views of the NIH.

Received: December 18, 2017
Accepted: April 13, 2018
Published: May 24, 2018

Web Resources

1000 Genomes, http://www.internationalgenome.org/
Baylor Genetics Laboratory, http://bmgl.com/
ClinVar, https://www.ncbi.nlm.nih.gov/clinvar/
Cufflinks, http://cufflinks.cbcb.umd.edu
DECIPHER, https://decipher.sanger.ac.uk/
ExAC Browser, http://exac.broadinstitute.org/
GenBank, http://www.ncbi.nlm.nih.gov/genbank/
GeneMatcher, https://genematcher.org/
GnomAD, http://gnomad.broadinstitute.org/
HTseq, http://www-huber.embl.de
Integrative Genomics Viewer (IGV), http://software.broadinstitute.org/software/igv
MutationTaster, http://www.mutationtaster.org/
NHLBI Exome Sequencing Project (ESP) Exome Variant Server, http://evs.gs.washington.edu/EVS/
OMIM, http://www.omim.org/
PolyPhen-2, http://genetics.bwh.harvard.edu/pph2/
Primer3, http://biotools.umassmed.edu/bioapps/primer3_www.cgi
UCSC Genome Browser, https://genome.ucsc.edu/

References

1. Bousfiha, A., Jeddane, L., Al-Herz, W., Ailal, F., Casanova, J.L., Chatila, T., Conley, M.E., Cunningham-Rundles, C., Etzioni, A., Franco, J.L., et al. (2015). The 2015 IUIS Phenotypic Classification for Primary Immunodeficiencies. J. Clin. Immunol. *35*, 727–738.
2. Casanova, J.L. (2015). Severe infectious diseases of childhood as monogenic inborn errors of immunity. Proc. Natl. Acad. Sci. USA *112*, E7128–E7137.
3. Pathak, S., McDermott, M.F., and Savic, S. (2017). Autoinflammatory diseases: update on classification diagnosis and management. J. Clin. Pathol. *70*, 1–8.
4. Brehm, A., Liu, Y., Sheikh, A., Marrero, B., Omoyinmi, E., Zhou, Q., Montealegre, G., Biancotto, A., Reinhardt, A., Almeida de Jesus, A., et al. (2015). Additive loss-of-function proteasome subunit mutations in CANDLE/PRAAS patients promote type I IFN production. J. Clin. Invest. *125*, 4196–4211.
5. Oda, H., and Kastner, D.L. (2017). Genomics, Biology, and Human Illness: Advances in the Monogenic Autoinflammatory Diseases. Rheum. Dis. Clin. North Am. *43*, 327–345.
6. Manthiram, K., Zhou, Q., Aksentijevich, I., and Kastner, D.L. (2017). The monogenic autoinflammatory diseases define new pathways in human innate immunity and inflammation. Nat. Immunol. *18*, 832–842.
7. Feist, E., Burmester, G.R., and Krüger, E. (2016). The proteasome - victim or culprit in autoimmunity. Clin. Immunol. *172*, 83–89.
8. Gatz, S.A., Salles, D., Jacobsen, E.M., Dörk, T., Rausch, T., Aydin, S., Surowy, H., Volcic, M., Vogel, W., Debatin, K.M., et al. (2016). *MCM3AP* and *POMP* Mutations Cause a DNA-Repair and DNA-Damage-Signaling Defect in an Immunodeficient Child. Hum. Mutat. *37*, 257–268.
9. Witt, E., Zantopf, D., Schmidt, M., Kraft, R., Kloetzel, P.M., and Krüger, E. (2000). Characterisation of the newly identified human Ump1 homologue POMP and analysis of LMP7(beta 5i) incorporation into 20S proteasomes. J. Mol. Biol. *301*, 1–9.
10. Budenholzer, L., Cheng, C.L., Li, Y., and Hochstrasser, M. (2017). Proteasome Structure and Assembly. J. Mol. Biol. *429*, 3500–3524.
11. Hoefer, M.M., Boneberg, E.M., Grotegut, S., Kusch, J., and Illges, H. (2006). Possible tetramerisation of the proteasome maturation factor POMP/proteassemblin/hUmp1 and its subcellular localisation. Int. J. Biol. Macromol. *38*, 259–267.
12. Burri, L., Höckendorff, J., Boehm, U., Klamp, T., Dohmen, R.J., and Lévy, F. (2000). Identification and characterization of a mammalian protein interacting with 20S proteasome precursors. Proc. Natl. Acad. Sci. USA *97*, 10348–10353.
13. Heink, S., Ludwig, D., Kloetzel, P.M., and Krüger, E. (2005). IFN-gamma-induced immune adaptation of the proteasome system is an accelerated and transient response. Proc. Natl. Acad. Sci. USA *102*, 9241–9246.
14. Fricke, B., Heink, S., Steffen, J., Kloetzel, P.M., and Krüger, E. (2007). The proteasome maturation protein POMP facilitates major steps of 20S proteasome formation at the endoplasmic reticulum. EMBO Rep. *8*, 1170–1175.
15. Seifert, U., and Krüger, E. (2008). Remodelling of the ubiquitin-proteasome system in response to interferons. Biochem. Soc. Trans. *36*, 879–884.
16. Dahlmann, B. (2016). Mammalian proteasome subtypes: Their diversity in structure and function. Arch. Biochem. Biophys. *591*, 132–140.
17. Moebius, J., van den Broek, M., Groettrup, M., and Basler, M. (2010). Immunoproteasomes are essential for survival and expansion of T cells in virus-infected mice. Eur. J. Immunol. *40*, 3439–3449.
18. de Graaf, N., van Helden, M.J., Textoris-Taube, K., Chiba, T., Topham, D.J., Kloetzel, P.M., Zaiss, D.M., and Sijts, A.J. (2011). PA28 and the proteasome immunosubunits play a central and independent role in the production of MHC class I-binding peptides in vivo. Eur. J. Immunol. *41*, 926–935.
19. Sijts, E.J., and Kloetzel, P.M. (2011). The role of the proteasome in the generation of MHC class I ligands and immune responses. Cell. Mol. Life Sci. *68*, 1491–1502.
20. Seifert, U., Bialy, L.P., Ebstein, F., Bech-Otschir, D., Voigt, A., Schröter, F., Prozorovski, T., Lange, N., Steffen, J., Rieger, M., et al. (2010). Immunoproteasomes preserve protein homeostasis upon interferon-induced oxidative stress. Cell *142*, 613–624.
21. Mégarbané, A., Sanders, A., Chouery, E., Delague, V., Medlej-Hashim, M., and Torbey, P.H. (2002). An unknown autoinflammatory syndrome associated with short stature and dysmorphic features in a young boy. J. Rheumatol. *29*, 1084–1087.
22. Dahlqvist, J., Klar, J., Tiwari, N., Schuster, J., Törmä, H., Badhai, J., Pujol, R., van Steensel, M.A., Brinkhuizen, T., Gijezen, L., et al. (2010). A single-nucleotide deletion in the POMP 5′ UTR causes a transcriptional switch and altered epidermal proteasome distribution in KLICK genodermatosis. Am. J. Hum. Genet. *86*, 596–603.
23. Dahlqvist, J., Törmä, H., Badhai, J., and Dahl, N. (2012). siRNA silencing of proteasome maturation protein (*POMP*) activates

the unfolded protein response and constitutes a model for KLICK genodermatosis. PLoS ONE *7*, e29471.
24. Tosato, G., and Cohen, J.I. (2007). Generation of Epstein-Barr Virus (EBV)-immortalized B cell lines. Curr. Protoc. Immunol. *Chapter 7*, 22.
25. Lupski, J.R., Gonzaga-Jauregui, C., Yang, Y., Bainbridge, M.N., Jhangiani, S., Buhay, C.J., Kovar, C.L., Wang, M., Hawes, A.C., Reid, J.G., et al. (2013). Exome sequencing resolves apparent incidental findings and reveals further complexity of *SH3TC2* variant alleles causing Charcot-Marie-Tooth neuropathy. Genome Med. *5*, 57.
26. Schindelin, J., Arganda-Carreras, I., Frise, E., Kaynig, V., Longair, M., Pietzsch, T., Preibisch, S., Rueden, C., Saalfeld, S., Schmid, B., et al. (2012). Fiji: an open-source platform for biological-image analysis. Nat. Methods *9*, 676–682.
27. Groot, N., de Graeff, N., Avcin, T., Bader-Meunier, B., Dolezalova, P., Feldman, B., Kenet, G., Koné-Paut, I., Lahdenne, P., Marks, S.D., et al. (2017). European evidence-based recommendations for diagnosis and treatment of paediatric antiphospholipid syndrome: the SHARE initiative. Ann. Rheum. Dis. *76*, 1637–1641.
28. Nagy, E., and Maquat, L.E. (1998). A rule for termination-codon position within intron-containing genes: when nonsense affects RNA abundance. Trends Biochem. Sci. *23*, 198–199.
29. Kurosaki, T., and Maquat, L.E. (2016). Nonsense-mediated mRNA decay in humans at a glance. J. Cell Sci. *129*, 461–467.
30. Steffen, J., Seeger, M., Koch, A., and Krüger, E. (2010). Proteasomal degradation is transcriptionally controlled by *TCF11* via an ERAD-dependent feedback loop. Mol. Cell *40*, 147–158.
31. Oslowski, C.M., and Urano, F. (2011). Measuring ER stress and the unfolded protein response using mammalian tissue culture system. Methods Enzymol. *490*, 71–92.
32. Miller, J.N., and Pearce, D.A. (2014). Nonsense-mediated decay in genetic disease: friend or foe? Mutat. Res. Rev. Mutat. Res. *762*, 52–64.
33. Bondurand, N., Dastot-Le Moal, F., Stanchina, L., Collot, N., Baral, V., Marlin, S., Attie-Bitach, T., Giurgea, I., Skopinski, L., Reardon, W., et al. (2007). Deletions at the *SOX10* gene locus cause Waardenburg syndrome types 2 and 4. Am. J. Hum. Genet. *81*, 1169–1185.
34. Inoue, K., Khajavi, M., Ohyama, T., Hirabayashi, S., Wilson, J., Reggin, J.D., Mancias, P., Butler, I.J., Wilkinson, M.F., Wegner, M., and Lupski, J.R. (2004). Molecular mechanism for distinct neurological phenotypes conveyed by allelic truncating mutations. Nat. Genet. *36*, 361–369.
35. White, J.J., Mazzeu, J.F., Hoischen, A., Bayram, Y., Withers, M., Gezdirici, A., Kimonis, V., Steehouwer, M., Jhangiani, S.N., Muzny, D.M., et al.; Baylor-Hopkins Center for Mendelian Genomics (2016). *DVL3* Alleles Resulting in a -1 Frameshift of the Last Exon Mediate Autosomal-Dominant Robinow Syndrome. Am. J. Hum. Genet. *98*, 553–561.
36. Xia, F., Bainbridge, M.N., Tan, T.Y., Wangler, M.F., Scheuerle, A.E., Zackai, E.H., Harr, M.H., Sutton, V.R., Nalam, R.L., Zhu, W., et al. (2014). De novo truncating mutations in *AHDC1* in individuals with syndromic expressive language delay, hypotonia, and sleep apnea. Am. J. Hum. Genet. *94*, 784–789.
37. Ben-Shachar, S., Khajavi, M., Withers, M.A., Shaw, C.A., van Bokhoven, H., Brunner, H.G., and Lupski, J.R. (2009). Dominant versus recessive traits conveyed by allelic mutations - to what extent is nonsense-mediated decay involved? Clin. Genet. *75*, 394–400.
38. Bayram, Y., White, J.J., Elcioglu, N., Cho, M.T., Zadeh, N., Gedikbasi, A., Palanduz, S., Ozturk, S., Cefle, K., Kasapcopur, O., et al.; Baylor-Hopkins Center for Mendelian Genomics (2017). *REST* Final-Exon-Truncating Mutations Cause Hereditary Gingival Fibromatosis. Am. J. Hum. Genet. *101*, 149–156.
39. Jansen, S., Geuer, S., Pfundt, R., Brough, R., Ghongane, P., Herkert, J.C., Marco, E.J., Willemsen, M.H., Kleefstra, T., Hannibal, M., et al.; Deciphering Developmental Disorders Study (2017). De Novo Truncating Mutations in the Last and Penultimate Exons of *PPM1D* Cause an Intellectual Disability Syndrome. Am. J. Hum. Genet. *100*, 650–658.
40. Burrage, L.C., Charng, W.L., Eldomery, M.K., Willer, J.R., Davis, E.E., Lugtenberg, D., Zhu, W., Leduc, M.S., Akdemir, Z.C., Azamian, M., et al. (2015). De Novo *GMNN* Mutations Cause Autosomal-Dominant Primordial Dwarfism Associated with Meier-Gorlin Syndrome. Am. J. Hum. Genet. *97*, 904–913.
41. Boisson, B., Quartier, P., and Casanova, J.L. (2015). Immunological loss-of-function due to genetic gain-of-function in humans: autosomal dominance of the third kind. Curr. Opin. Immunol. *32*, 90–105.
42. Gerbracht, J.V., Boehm, V., and Gehring, N.H. (2017). Plasmid transfection influences the readout of nonsense-mediated mRNA decay reporter assays in human cells. Sci. Rep. *7*, 10616.
43. Sasaki, K., Hamazaki, J., Koike, M., Hirano, Y., Komatsu, M., Uchiyama, Y., Tanaka, K., and Murata, S. (2010). *PAC1* gene knockout reveals an essential role of chaperone-mediated 20S proteasome biogenesis and latent 20S proteasomes in cellular homeostasis. Mol. Cell. Biol. *30*, 3864–3874.
44. Kock, M., Nunes, M.M., Hemann, M., Kube, S., Dohmen, R.J., Herzog, F., Ramos, P.C., and Wendler, P. (2015). Proteasome assembly from 15S precursors involves major conformational changes and recycling of the Pba1-Pba2 chaperone. Nat. Commun. *6*, 6123.
45. Veitia, R.A. (2007). Exploring the molecular etiology of dominant-negative mutations. Plant Cell *19*, 3843–3851.
46. Veitia, R.A. (2009). Dominant negative factors in health and disease. J. Pathol. *218*, 409–418.
47. Sotzny, F., Schormann, E., Kühlewindt, I., Koch, A., Brehm, A., Goldbach-Mansky, R., Gilling, K.E., and Krüger, E. (2016). TCF11/Nrf1-Mediated Induction of Proteasome Expression Prevents Cytotoxicity by Rotenone. Antioxid. Redox Signal. *25*, 870–885.
48. Zhang, X., Schulz, R., Edmunds, S., Krüger, E., Markert, E., Gaedcke, J., Cormet-Boyaka, E., Ghadimi, M., Beissbarth, T., Levine, A.J., et al. (2015). MicroRNA-101 Suppresses Tumor Cell Proliferation by Acting as an Endogenous Proteasome Inhibitor via Targeting the Proteasome Assembly Factor POMP. Mol. Cell *59*, 243–257.
49. Koerner, J., Brunner, T., and Groettrup, M. (2017). Inhibition and deficiency of the immunoproteasome subunit LMP7 suppress the development and progression of colorectal carcinoma in mice. Oncotarget *8*, 50873–50888.
50. Hensley, S.E., Zanker, D., Dolan, B.P., David, A., Hickman, H.D., Embry, A.C., Skon, C.N., Grebe, K.M., Griffin, T.A., Chen, W., et al. (2010). Unexpected role for the immunoproteasome subunit LMP2 in antiviral humoral and innate immune responses. J. Immunol. *184*, 4115–4122.